

May, 2022

# Leptophilic Gauge Bosons at Lepton Beam Dump Experiments

Takeo Moroi and Atsuya Niki

*Department of Physics, University of Tokyo, Tokyo 113-0033, Japan*

## Abstract

It has been recently known that we can use beams of future lepton colliders, the International Linear Collider (ILC), the Compact Linear Collider (CLIC), and the muon collider, for beam dump experiment if a shield and a detector are installed behind the beam dump. We study the prospect of searching for leptophilic gauge bosons (LGBs) in association with  $U(1)_{L_e-L_\mu}$ ,  $U(1)_{L_e-L_\tau}$ , and  $U(1)_{L_\mu-L_\tau}$  gauge symmetries at such lepton beam dump experiments. We perform a detailed calculation of the event rates of the LGB events, taking into account bremsstrahlung and pair-annihilation processes. We show that the lepton beam dump experiments at future lepton colliders can reach parameter regions which are not been covered.

# 1 Introduction

While the standard model (SM) successfully explains most of the electroweak-scale phenomena, it is widely believed that there exists physics beyond the standard model (BSM). To search for the BSM particles, the high energy collider experiments with lepton beam, such as the International Linear Collider (ILC) [1, 2, 3, 4, 5, 6], the Compact Linear Collider (CLIC) [7], and the muon collider [8], are highly appreciated as prominent candidates of future collider experiments. One advantage of lepton colliders is that elementary processes at the interaction point and the background are well understood, so the lepton collider experiments are suited for the precision test of the high energy physics like Higgs properties.

In recent years, it has been pointed out that the high-energy lepton collider experiments can be also used for beam dump experiments, a kind of fixed target experiment [9, 10]. In this experiment, beam is injected into a beam dump, then new particles are produced through the interactions between the beam and the material in the beam dump. Since one of the initial states is a fixed target, the luminosity is greatly increased and the beam dump experiment has an advantage to search for feebly interacting particles compared to the collider experiments. In addition, the beam dump experiment at the future lepton collider has several advantages compared to fixed target experiments in the past: high energy beam ( $> \mathcal{O}(100)$  GeV) and a large amount of the initial-state leptons. Due to these advantages, it has been shown that the beam dump experiment using the ILC beam can cover the parameter regions of long-lived BSM particles where the previous experiments could not explore [9, 11, 12, 13].

Among various possibilities of BSM physics, in this paper, we concentrate on gauge bosons in association with new  $U(1)$  gauge symmetries coupled to the difference of the lepton-family numbers,  $U(1)_{Le-L\mu}$ ,  $U(1)_{Le-L\tau}$ , and  $U(1)_{L\mu-L\tau}$  [14, 15, 16, 17]. These new  $U(1)$  gauge symmetries can be introduced without quantum anomaly. We call the gauge bosons of our interest as leptophilic gauge bosons (LGBs). The phenomenology of leptophilic  $U(1)$  gauge symmetry have been intensively discussed; relevant subjects include neutrino physics [18, 19, 20, 21, 22], muon anomalous magnetic moment [23, 24], dark matter [25, 26, 27], and so on. These LGBs can be long-lived in some parameter regions so they may be detected by the beam dump experiment. Ref. [13] considered the search for LGBs in the ILC beam dump experiment and show that the ILC beam dump experiment can explore the parameter region which is still viable. In particular, for the case of  $U(1)_{L\mu-L\tau}$ , the ILC beam dump experiment can cover part of the regions where the LGB alleviates the Hubble tension [28]. In Ref. [13], only the effect of the  $e^-$  beam particle was taken into account. However, there can occur scattering processes using the secondary  $e^\pm$ 's and  $\mu^\pm$ 's. In addition, the LGB can be produced via the annihilation process between the energetic beam or secondary  $e^+$  and the atomic  $e^-$ . These processes, which also contribute to the production of the LGB, are considered in the present study.

In this paper, we consider the possibility to search for the LGBs with the beam dump experiments using energetic beams of lepton colliders. We study in detail the production processes of LGBs as well as the detection efficiency and obtain the discovery reach. We

take into account the production processes of LGBs which have not been considered in the previous analysis: the secondary  $e^\pm$  and  $\mu^\pm$  bremsstrahlung process and the positron  $e^+$  annihilation process. The cross section of the annihilation process can be larger than that of the bremsstrahlung process in some parameter space, so the sensitivity can be improved by this process. Furthermore, since the LGB of  $U(1)_{L_\mu-L_\tau}$  model does not couple to  $e^\pm$  at tree level, the effects of secondary  $\mu^\pm$  may be non-negligible. We also consider the search for LGBs using the muon beam of the muon colliders.

The organization of this paper is as follows. We introduce the  $U(1)_{L_i-L_j}$  ( $i, j = e, \mu, \tau$ ) models in Sec. 2 and the beam dump experiment in Sec. 3. Then we explain the calculation of the event rate in Sec. 4. We show the discovery reaches for the each model in the lepton beam dump experiments in Sec. 5 and Sec. 6. Sec. 7 is devoted for summary and discussion.

## 2 Model

We consider the  $U(1)_{L_i-L_j}$  ( $i, j = e, \mu, \tau$ ) models, where  $L_i$  is the lepton  $i$  number. The charge assignment for the lepton  $\ell$  is

$$Q_\ell \equiv \begin{cases} 1 & : \ell = i, \\ -1 & : \ell = j, \\ 0 & : \text{otherwise.} \end{cases} \quad (2.1)$$

These  $U(1)$  extensions are gauge anomaly free without new particles, and we do not introduce new matter particles charged under the  $U(1)_{L_i-L_j}$  symmetry for simplicity.<sup>#1</sup> Furthermore, we assume that the  $U(1)_{L_i-L_j}$  symmetry is spontaneously broken and that the LGB is massive; the Higgs field responsible for the spontaneous breaking of  $U(1)_{L_i-L_j}$  is assumed to be heavy enough so that it does not affect the following discussion. Then the relevant part of the Lagrangian for our study is given by

$$\begin{aligned} \mathcal{L} = & -\frac{1}{4}F_{\mu\nu}F^{\mu\nu} - \frac{1}{4}X_{\mu\nu}X^{\mu\nu} - \frac{\epsilon_0}{2}X_{\mu\nu}F^{\mu\nu} + \frac{1}{2}m_A^2 A'_\mu A'^\mu + eA_\mu J_{EM}^\mu \\ & + g'A'_\mu J_{DS}^\mu + g'A'_\mu \sum_{\ell=e,\mu,\tau} Q_\ell (\bar{\ell}\gamma^\mu \ell + \bar{\nu}_\ell \gamma^\mu P_L \nu_\ell) + \cdots, \end{aligned} \quad (2.2)$$

where  $P_L \equiv \frac{1}{2}(1 - \gamma_5)$ ,  $A_\mu$  ( $A'_\mu$ ) is the photon (the LGB) and  $F_{\mu\nu}$  ( $X_{\mu\nu}$ ) is its field strength.

In Eq. (2.2), the third term is the tree-level kinetic mixing term. There is also a 1-loop contribution to the kinetic mixing, as is shown in Fig. 1. Then, the effective mixing parameter, which is used to calculate the decay rate of the LGB, is given by

$$\epsilon \equiv \epsilon_0 + \Delta\epsilon, \quad (2.3)$$

---

<sup>#1</sup>When we introduce new particle which is charged under the  $U(1)_{L_i-L_j}$  symmetry and singlet of the SM symmetries, this new particles can be a dark matter candidate [25, 26, 27]. The existence of this new particle may affect the sensitivity of the LGB in the beam dump experiment because the LGB may decay into this new particle, which cannot be detected. To search for this kind of particles in the dark sector, we should use the other type of the fixed target experiment setup, like LDMX [29].

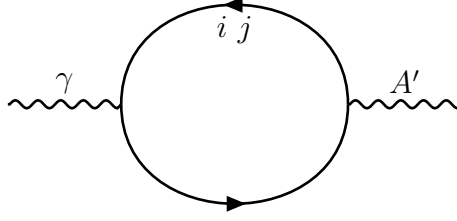


Figure 1: 1-loop induced kinetic mixing between photon and leptophilic gauge boson via exchanging the corresponding charged leptons.

where

$$\Delta\epsilon = \frac{eg'}{2\pi^2} \int_0^1 dx \, x(1-x) \ln \frac{m_j^2 - m_{A'}^2 x(1-x)}{m_i^2 - m_{A'}^2 x(1-x)}. \quad (2.4)$$

After diagonalizing the kinetic terms of gauge bosons, the Lagrangian contains the following interaction:

$$\mathcal{L} \ni -\epsilon e A'_\mu J_{EM}^\mu. \quad (2.5)$$

In order to reduce the unknown parameter, we set the tree-level kinetic mixing parameter to be zero, *i.e.*,  $\epsilon_0 = 0$ . Then the interactions between the LGB and the electromagnetic current suffer the 1-loop suppression.

The interactions between LGB and SM particles can be denoted as

$$\mathcal{L} \ni - \sum_{\ell} (g_{\ell} \bar{\ell} A' \ell + g_{\nu_{\ell}} \bar{\nu}_{\ell} A' P_L \nu_{\ell}), \quad (2.6)$$

where

$$-g_i = g_j = g', \quad g_{\ell \neq i,j} = \epsilon e, \quad -g_{\nu_i} = g_{\nu_j} = g', \quad g_{\nu_{\ell \neq i,j}} = 0. \quad (2.7)$$

In the case of the  $U(1)_{L_e-L_\mu}$  and  $U(1)_{L_e-L_\tau}$  models, the LGB couples with  $e$  via the gauge interaction. On the other hand, in the case of the  $U(1)_{L_\mu-L_\tau}$  model, the LGB couples with  $\mu$  and  $\tau$  flavor leptons at tree level and with  $e$  at only loop level.

Through these interactions, the LGB can decay into the SM particles when the decay mode is kinematically allowed. The LGB's partial decay rates to the charged lepton pair are given by

$$\Gamma(A' \rightarrow \ell^+ \ell^-) = \begin{cases} \frac{g'^2}{12\pi} m_{A'} \sqrt{1 - \frac{4m_{\ell}^2}{m_{A'}^2}} \left(1 + \frac{2m_{\ell}^2}{m_{A'}^2}\right) & : \ell = i, j, \\ \frac{(\epsilon e)^2}{12\pi} m_{A'} \sqrt{1 - \frac{4m_l^2}{m_{A'}^2}} \left(1 + \frac{2m_l^2}{m_{A'}^2}\right) & : \text{otherwise,} \end{cases} \quad (2.8)$$

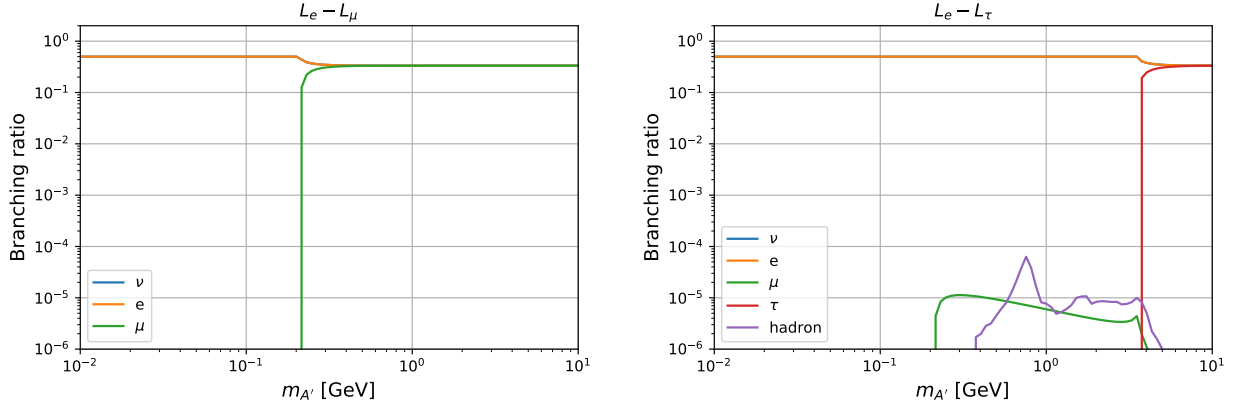
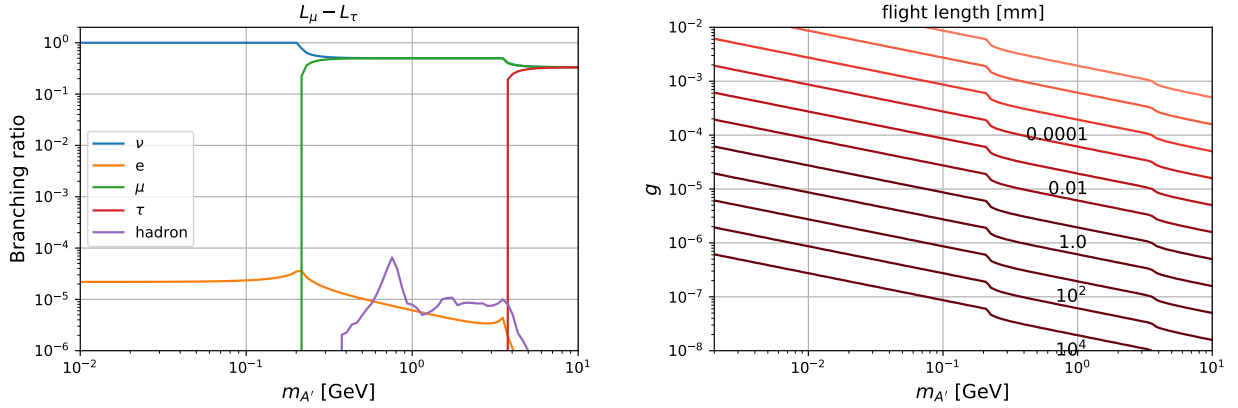


Figure 2: The branching ratios for the  $U(1)_{L_e-L_\mu}$  gauge boson (left) and the  $U(1)_{L_e-L_\tau}$  gauge boson (right). (Notice that the branching ratios for the  $e^\pm$  and the neutrino final states are very close and hence they are indistinguishable in the figures.)



(a) Branching Ratio

(b) Decay Length  $c\tau$  [mm]

Figure 3: The decay properties of the  $U(1)_{L_\mu-L_\tau}$  gauge boson. (a) the branching ratio (b) the decay length  $c\tau$ , where  $\tau$  is the lifetime.

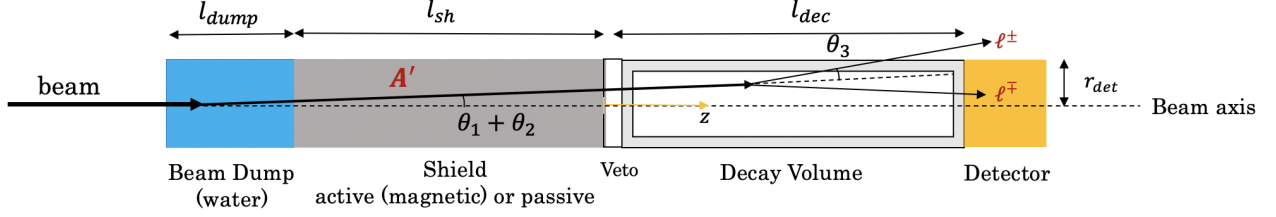


Figure 4: Rough sketch of the experimental setup of the lepton beam dump experiment.  $A'$  is the LGB and  $l^\pm$  is its decay particles.  $r_{det}$  is the radius of the detector.  $A'$  is produced at the beam dump ( $A'$  can be also produced in the shield by the secondary muon) and then it travels to the decay volume. In the decay volume,  $A'$  decays into a lepton pair  $\ell^+\ell^-$ . We observe this lepton pair at the detector.

while the partial decay rates to neutrino pair is given by

$$\Gamma(A' \rightarrow \nu_\ell \bar{\nu}_\ell) = \begin{cases} \frac{g'^2}{24\pi} m_{A'} & : \ell = i, j, \\ 0 & : \text{otherwise.} \end{cases} \quad (2.9)$$

Furthremore, the partial decay rate to hadron can be expressed as

$$\Gamma(A' \rightarrow \text{hadron}) = \Gamma(A' \rightarrow \mu^+ \mu^-) R(m_{A'}), \quad (2.10)$$

where  $R$  is the  $r$ -ratio [30, 31]. The branching ratio of the  $U(1)_{L_i-L_j}$  gauge bosons are shown in Fig. 2 and Fig. 3. In the case of the  $U(1)_{L_e-L_\mu}$  and  $U(1)_{L_e-L_\tau}$  models, the LGB decays into  $e^+e^-$  pair dominantly as well as neutrino pair and the branching ratio into  $e^+e^-$  pair is  $\mathcal{O}(0.1)$ . On the other hand, the LGB of the  $U(1)_{L_\mu-L_\tau}$  model couples with muon and tau flavor at tree level but that it interacts with electron flavor and quarks only via the loop effect. So the branching ratio of the decay modes to electron pair and hadrons are suppressed. In particular, when the LGB mass is less than twice of the muon mass, the possible final states of the LGB decay are  $e^+e^-$  pair and neutrino pair. As is explained, the decay rate into  $e^+e^-$  pair is suppressed and most of the decay products are invisible neutrinos in this mass range. This makes it difficult to find light LGB in  $U(1)_{L_\mu-L_\tau}$  model.

### 3 Beam Dump Experiment

In this section, we explain the experimental setup of the lepton beam dump experiment. In  $e^+e^-$  linear colliders such as the ILC and the CLIC, the beams passing through the interaction point are expected to be dumped into the beam dumps. Then, the beam dump can be used as a target for the beam dump experiment if additional equipment is installed behind the beam dump. In the following, we consider such a possibility.

The sketch of the setup is shown in Fig. 4. Behind the beam dump, a shield, veto and the decay volume with particle detector are installed; the lengths of the beam dump, the shield, and the decay volume are denoted as  $L_{dump}$ ,  $L_{shield}$ , and  $L_{dec}$ , respectively. The shield is intended to eliminate muon and other backgrounds.<sup>#2</sup> Once a LGB is produced in the beam dump, it may pass through the beam dump and the shield, reaching to the decay volume. If the LGB decays into visible particles in the decay volume, they may be observed by the detector. Hereafter, we assume that charged SM particles are fully blocked by the shield and that the background is negligible.

Before closing this section, we comment on the mean free path of the LGB in the beam dump and the shield. In our analysis, we consider the case that the beam energy is a much larger than the LGB mass  $m_{A'}$ . In this case, the mean free path of the LGB can be obtained by rescaling that of the photon. When the LGB energy is larger than 1 GeV, the LGB mean free path is estimated to be  $L \sim \frac{e^2}{g'^2}$  cm in the lead [31]. As we will see, we will investigate the region of  $g' < 10^{-4}$ , for which the mean free path is much larger than 100 m. Then, with the experimental setup of our choice, we can safely neglect the interaction of the LGB in the beam dump and shield.

## 4 Event Rate

In this section, we explain how to calculate the event rate in the beam dump experiment. The event rate  $N$  is expressed as

$$N = N_l N_{target} \sigma \mathcal{A}, \quad (4.1)$$

where  $N_l$  is the number of the leptons injected into the beam dump per time,  $N_{target}$  is the effective number of particles in the target,  $\sigma$  is the cross section for the production process and  $\mathcal{A}$  is the acceptance of the detection. More details will be discussed in the following.

### 4.1 Production process

In this subsection, we discuss the production processes and the cross sections of the LGBs. In the  $e^\pm$  beam dump experiment, the candidates of the initial-state particle are the beam  $e^\pm$  and the secondary  $e^\pm$ ,  $\mu^\pm$ , and  $\gamma$ . For the LGB production, the bremsstrahlung process by the charged particle and the annihilation process by the incoming positron and the atomic electron are the dominant production processes (see Fig. 5).

#### 4.1.1 Bremsstrahlung

The bremsstrahlung is the radiation process from the charged particles propagating in the matter. The diagram is shown in Fig. 5 (a). We calculate the cross section using the im-

---

<sup>#2</sup>We can consider two types of shields, active shield or passive shield. The active shield is the SHiP-like shield [32], in which we use the magnetic field to remove the muons. The passive shield is just an enough-long lead shield to stop the muons. Using this shield the secondary muons can also produce the new gauge bosons.

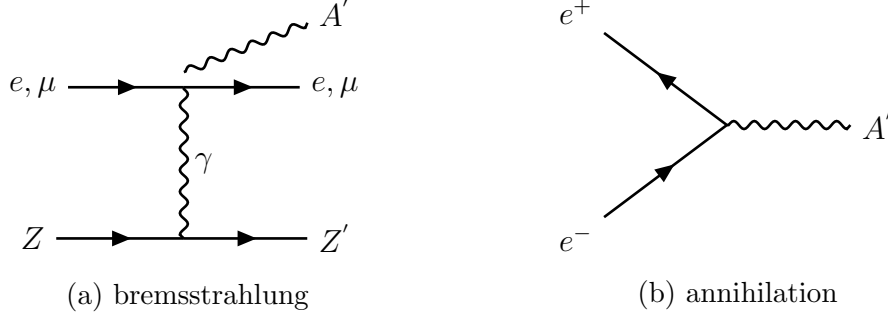


Figure 5: Production processes in the lepton beam dump experiment.  $A'$  is a LGB and  $Z, Z'$  are the nucleus.

proved Weizsacker-Williams approximation [33, 34, 35]. The cross section with the incoming charged particles  $\ell^\pm (= e, \mu)$  is<sup>#3</sup>

$$\frac{d\sigma(\ell + Z \rightarrow \ell + Z' + A')}{dx d\cos\theta_{A'}} = \frac{2\alpha^2 g_\ell^2}{\pi} \chi \beta_{A'} E_\ell^2 x \left[ \frac{1 - x + \frac{1}{2}x^2}{U^2} + \frac{(1-x)^2(m_{A'}^2 + 2m_\ell^2)}{U^4} \left( m_{A'}^2 - \frac{x}{1-x}U + \frac{x^2}{1-x}m_\ell^2 \right) \right], \quad (4.2)$$

where  $E_{A'}$  ( $E_\ell$ ) is the energy of the LGB (the charged particle  $\ell^\pm$ ),  $\theta_{A'}$  is the angle of the LGB from the propagation direction of  $\ell^\pm$ , and

$$x = \frac{E_{A'}}{E_\ell} \quad (4.3)$$

$$\beta_{A'} = \sqrt{1 - \frac{m_{A'}^2}{E_{A'}^2}} \quad (4.4)$$

$$U(x, \theta_{A'}) \equiv E_\ell^2 \theta_{A'}^2 x + m_{A'}^2 \frac{1-x}{x} + m_\ell^2 x. \quad (4.5)$$

In addition,  $\chi$  is the effective photon flux:

$$\chi = \int_{\tilde{t}_{min}}^{\tilde{t}_{max}} d\tilde{t} \frac{\tilde{t} - \tilde{t}_{min}}{\tilde{t}^2} G_2(\tilde{t}), \quad (4.6)$$

where the elastic and inelastic form factor of the target of the mass number  $A$  is given by

$$G_2(\tilde{t}) = \left( \frac{a^2 \tilde{t}}{1 + a^2 \tilde{t}} \right)^2 \left( \frac{1}{1 + \tilde{t}/d} \right)^2 Z^2 + \left( \frac{a'^2 \tilde{t}}{1 + a'^2 \tilde{t}} \right)^2 \left( \frac{1 + (\mu_p^2 - 1)\tilde{t}/4m_p^2}{(1 + \tilde{t}d')^4} \right)^2 Z, \quad (4.7)$$

<sup>#3</sup>The approximation for the cross section is a little bit different from the  $e^\pm$  bremsstrahlung cross section [36]. This is because  $m_\mu$  is not necessary smaller than the LGB mass  $m_{A'}$ .



with  $m_p$  being the proton mass,  $a = 111Z^{-\frac{1}{3}}/m_e$ ,  $d = 0.146 \text{ GeV}^2 A^{-\frac{2}{3}}$ ,  $a' = 773Z^{-\frac{2}{3}}/m_e$ ,  $d = 0.71 \text{ GeV}^2$ , and  $\mu_p = 2.79$ . We set  $t_{min} \simeq \left(\frac{m_{A'}^2}{2E_\ell}\right)^2$  and  $t_{max} \simeq m_{A'}^2 + m_\ell^2$  [37, 38].

The cross section is enhanced in the collinear region  $\theta_{A'} \sim 0$ . Furthermore, the LGB is detected only when the LGB flies collinearly to the beam axis. Due to these reasons, we concentrate on the case that  $\theta_{A'}$  is very small. Then, integrating the differential cross section for  $\theta_{min} \leq \theta_{A'} \leq \theta_{max}$ , we obtain

$$\begin{aligned} \frac{d\sigma}{dx} = & \frac{2\alpha^2 g_\ell^2}{\pi} \chi_{\beta_{A'}} \left[ \frac{1-x+\frac{1}{2}x^2}{E_\ell^2 x} \frac{1}{2} \left( \frac{1}{\theta_{min}^2 + \eta} - \frac{1}{\theta_{max}^2 + \eta} \right) \right. \\ & + \frac{(1-x)^2(m_{A'}^2 + 2m_\ell^2)m_{A'}^2}{(E_\ell^2 x)^3} \frac{1}{6} \left( \frac{1}{(\theta_{min}^2 + \eta)^3} - \frac{1}{(\theta_{max}^2 + \eta)^3} \right) \\ & - \frac{(1-x)x(m_{A'}^2 + 2m_\ell^2)}{(E_\ell^2 x)^2} \frac{1}{4} \left( \frac{1}{(\theta_{min}^2 + \eta)^2} - \frac{1}{(\theta_{max}^2 + \eta)^2} \right) \\ & \left. + \frac{(1-x)x^2(m_{A'}^2 + 2m_\ell^2)m_\ell^2}{(E_\ell^2 x)^3} \frac{1}{6} \left( \frac{1}{(\theta_{min}^2 + \eta)^3} - \frac{1}{(\theta_{max}^2 + \eta)^3} \right) \right], \end{aligned} \quad (4.8)$$

where  $\eta = \frac{m_{A'}^2}{E_\ell^2} \frac{1-x}{x} + \frac{m_\ell^2}{E_\ell^2}$ .

#### 4.1.2 Annihilation

The incoming positron (beam particle or secondary particle) and the electron in the atom can annihilate into the LGB, as is shown in Fig. 5 (b). The cross section for the annihilation process  $e^+e^- \rightarrow A' \rightarrow \ell^+\ell^-$  is

$$\sigma_{ann}^\ell = \frac{g_e^2 g_\ell^2 E_{CM}^2}{12\pi[(E_{CM}^2 - m_{A'}^2)^2 + m_{A'}^2 \Gamma_{A'}^2]} \sqrt{1 - 4\frac{m_\ell^2}{E_{CM}^2}} \left( 1 + 2\frac{m_\ell^2}{E_{CM}^2} \right), \quad (4.9)$$

where  $E_{CM}$  is the center of mass energy. If the LGB is long-lived, the narrow-width approximation can be used:

$$\sigma_{ann}^\ell = \frac{g_e^2 g_\ell^2}{24} \frac{E_{CM}^2}{m_{A'}^2 \Gamma_{A'}} \sqrt{1 - 4\frac{m_\ell^2}{E_{CM}^2}} \left( 1 + 2\frac{m_\ell^2}{E_{CM}^2} \right) \delta(E_{CM} - m_{A'}). \quad (4.10)$$

## 4.2 Experimental acceptance

The LGB can be produced in the beam dump through the bremsstrahlung and the annihilation process, as we discussed in the previous subsection. However, not all of the LGBs can be detected. There are two reasons: one is that not all of the LGB can travel through the dump and the shield, and another is that the detector is assumed to be installed in the very forward direction.<sup>#4</sup> We estimate the experimental acceptance (corresponding to the

<sup>#4</sup>We also check the situation when the detector is installed on every side of the decay volume and the sensitivity becomes better, as expected [39].

detection efficiency of the LGB produced in the dump) as

$$\mathcal{A} = \frac{1}{L_{A'}} e^{-(L_{dump} + L_{sh})/L_{A'}} \int_0^{L_{dec}} dz e^{-z/L_{A'}} \Theta(r_{det} - r_{\perp}(z)), \quad (4.11)$$

where  $z$  is the distance from the shield to the decay point of the LGB,  $r_{det}$  is the radius of the detector (as shown in Fig. 4), and

$$L_{A'} = \frac{p_{A'}}{\Gamma_{A'} m_{A'}}. \quad (4.12)$$

In addition,  $r_{\perp}(z)$  is the distance of the final state particle from the beam axis at the position of the detector. We adopt an approximation that  $r_{\perp}(z)$  is estimated by using typical scattering and decay angles of the production; consequently, in our analysis,  $r_{\perp}(z)$  is calculated as a function of  $z$  (see below). Then, the theta function in Eq. (4.11) takes account of the angular acceptance. Estimation of  $r_{\perp}$  depends on the initial state particle:

- Incoming  $e^{\pm}$ : In this case, the production process mostly occurs at the front edge of the beam dump. Then, the  $r_{\perp}$  is estimated as

$$r_{\perp} \simeq (\theta_1 + \theta_2)(L_{dump} + L_{sh} + z) + (\theta_1 + \theta_2 + \theta_3)(L_{dec} - z), \quad (4.13)$$

where  $\theta_1$  is the  $e^{\pm}$  angle from the beam axis,  $\theta_2$  is  $A'$  angle from the propagation direction of  $e^{\pm}$ , and  $\theta_3$  is the angle between the propagation directions of  $A'$  and final state particle.<sup>#5</sup> Here the angles  $\theta_{1,2,3}$  are approximated by the typical values [40, 11]:

$$\theta_1 = 16 \text{ mrad} \cdot \text{GeV}/E_{e^{\pm}}, \quad (4.14)$$

$$\theta_2 = \begin{cases} \max\left(\frac{\sqrt{m_{A'} m_e}}{E_e}, \left(\frac{m_{A'}}{E_e}\right)^{\frac{3}{2}}\right), & \text{: bremsstrahlung} \\ 0 & \text{: annihilation,} \end{cases} \quad (4.15)$$

$$\theta_3 = \frac{\pi m_{A'}}{2E_{A'}}. \quad (4.16)$$

It is required that  $r_{\perp} < r_{det}$ , then we obtain the acceptance as

$$\mathcal{A}_e^{brem,ann} \simeq e^{-(L_{dump} + L_{sh})/L_{A'}} (e^{-z_{min}/L_{A'}} - e^{-L_{dec}/L_{A'}}), \quad (4.17)$$

where

$$z_{min} \equiv \frac{1}{\theta_3} [(\theta_1 + \theta_2)(L_{dump} + L_{sh}) + (\theta_1 + \theta_2 + \theta_3)L_{dec} - r_{det}]. \quad (4.18)$$

---

<sup>#5</sup>Since the angles  $\theta_{1,2,3}$  are independent, we may use the root mean square to estimate  $r_{\perp}$ . Eq. (4.13) assumes the worst case when the final state flies away from the beam axis, so our estimation is conservative. Ref. [12] used the root mean square to estimate  $r_{\perp}$ . We have checked that, even if we use the root mean square, results do not change significantly. In our analysis, we use Eq. (4.13) to simplify the calculation.

- Incoming  $\mu^\pm$ : Since the flight length of the muon is  $> \mathcal{O}(10)$  m in the lead shield, the production point of the LGB can not be approximated by the front edge of the beam dump as the incoming  $e^\pm$  case. We approximate the flight length of the muon in matter as

$$\delta_\mu = \frac{E_{\mu_0} - E_\mu}{\langle dE/dx \rangle},$$

where  $E_{\mu_0}$  ( $E_\mu$ ) is the energy of initial (attenuated) muon in the target. The energy-loss rate in lead is almost energy independent:  $\langle dE/dx \rangle \simeq 0.02$  GeV/cm.<sup>#6</sup> We neglect the energy loss of the muon in water. Then, we obtain  $r_\perp$  as

$$r_\perp \simeq \theta_1(L_{dump} + \delta_\mu) + (\theta_1 + \theta_2)(L_{shield} + z - \delta_\mu) + (\theta_1 + \theta_2 + \theta_3)(L_{dec} - z), \quad (4.19)$$

where  $\theta_1$  is the muon angle from the beam axis while  $\theta_{2,3}$  are the same as the  $e^\pm$  case. The typical value of  $\theta_1$  is

$$\theta_1 = \sqrt{\left(\frac{2m_\mu}{E_{\mu_0}}\right)^2 + \theta_0}, \quad (4.20)$$

where  $\theta_0$  is the standard variance of the angular distribution of the multiple coulomb scattering (see Ref. [11] for the concrete expression of  $\theta_0$ ). Consequently, we obtain

$$\mathcal{A}_e^\mu \simeq e^{-(L_{sh}-\delta_\mu)/L_{A'}} \left( e^{-z_{min}^\mu/L_{A'}} - e^{-L_{dec}/L_{A'}} \right), \quad (4.21)$$

where

$$z_{min}^\mu \equiv \frac{1}{\theta_3} [-\theta_2\delta_\mu + \theta_1 L_{dump} + (\theta_1 + \theta_2)L_{shield} + (\theta_1 + \theta_2 + \theta_3)L_{dec} - r_{det}]. \quad (4.22)$$

### 4.3 Event rate

The remaining quantities to calculate the event rate in Eq. (4.1) are  $N_l$  and  $N_{target}$ . The number of lepton in the beam  $N_l$  is determined by the experimental setup. For example,  $N_e$  in the ILC experiment is about  $4 \times 10^{21}$  per year [1, 2, 3, 4, 5].  $N_{target}$  is estimated by using the track length  $l_m$ , which is the total flight length of the particle  $m$  including the effects from the secondary particles:

$$N_{target}(E_m) = \sum_m \frac{N_{Avo}\rho}{A} \frac{dl_m}{dE_m}(E_m), \quad (4.23)$$

where  $N_{Avo}$  is the Avogadro number and  $\rho$  ( $A$ ) is the density (mass number) of the target.

---

<sup>#6</sup>For the relativistic muon with  $E_\mu < 1$  TeV, it can be approximated as a minimum ionizing particle (mip). This means that the energy loss of mip in the target is approximated by the minimum ionizing energy, that is, the energy loss is approximately energy independent.

Based on the discussion so far, we can calculate the event rate. For the event when the LGB is produced by the  $e^\pm$  bremsstrahlung process,

$$N_e^{brem} = B_{vis} N_e \frac{N_{Avo} \rho}{A} \int_{m_{A'} + m_e}^{E_{beam}} dE_e \int_{m_{A'}}^{E_e - m_e} dE_{A'} \sum_{e^\pm} \frac{dl_{e^\pm}}{dE_e} \frac{1}{E_e} \left[ \frac{d\sigma}{dx} \right]_{x=\frac{E_{A'}}{E_e}} \mathcal{A}_e^{brem}, \quad (4.24)$$

where  $B_{vis}$  is the branching ratio for the visible particles.<sup>#7</sup> For the event when the LGB is produced by the annihilation process,

$$N_e^{ann} = N_e \left( \frac{N_{Avo} \rho}{A} Z \right) \int_{m_{A'} + m_e}^{E_{beam}} dE_e \frac{dl_{e^+}}{dE_e} \sum_{\ell=e,\mu} \sigma_{ann}^\ell \Theta(E_{CM} - 2m_\ell) \mathcal{A}_e^{ann}. \quad (4.25)$$

For the event when the LGB is produced by the secondary  $\mu^\pm$  bremsstrahlung process,<sup>#8</sup>

$$N_\mu = B_{vis} N_e \frac{N_{Avo} \rho}{A} \int_{m_\mu}^{E_{beam}} dE_{\mu_0} \int_{m_{A'} + m_\mu}^{E_{\mu_0}} dE_\mu \int_{m_{A'}}^{E_\mu - m_e} dE_{A'} \frac{dl_\mu}{dE_\mu} \frac{dY_{\mu_0}}{dE_{\mu_0}} \frac{1}{E_\mu} \left[ \frac{d\sigma}{dx} \right]_{x=\frac{E_{A'}}{E_\mu}} \mathcal{A}_e^\mu, \quad (4.26)$$

where  $Y_{\mu_0}$  is the energy distribution function of muons in the target when the electron is injected [42]:

$$\frac{dY_{\mu_0}}{dE_{\mu_0}} = \frac{0.572 E_{beam}}{\ln(183 Z^{-1/3})} \left( \frac{m_e}{m_\mu} \right)^2 \left( \frac{1}{E_{\mu_0}^2} - \frac{1}{E_{beam}^2} \right). \quad (4.27)$$

## 5 The $e^\pm$ Beam Dump Experiment

In this section, we show the discovery reach for the LGB in the  $e^\pm$  beam dump experiment. Before showing the results, we summarize the concrete experimental setup adopted in this section:

- The target is  $H_2O$  in the beam dump and the length is  $L_{dump} = 11$  m ( $30X_0$ , with  $X_0$  being the radiation length).
- The shield is installed behind the beam dump. We assume zero background due to the shield. The shield length is assumed as  $L_{shield} = 50$  m.
- The decay volume is installed behind the shield. The length of the decay volume is assumed as  $L_{dec} = 50$  m.

<sup>#7</sup>In Eq. (4.24), the lower limit of  $E_{A'}$  is set to be  $m_{A'}$ . When  $m_{A'}$  is small,  $N^{(brem)}$  includes signals with soft final state particles and the event rate is overestimated in this calculation. When the energy cut at the detector is considered, signals with soft particles are rejected and the discovery reach is modified [41].

<sup>#8</sup>For the primary muon case, see Sec. 6.

- The detector is installed behind the decay volume. The radius of the detector is assumed as  $r_{det} = 2$  m.
- The ILC bunch train contains 1312 bunches and each bunch has  $2 \times 10^{10} e^\pm$ . The frequency of the dump of the bunch train is 5 Hz. Thus  $4 \times 10^{21} e^\pm$  are injected with a 1-year operation [1, 2, 3, 4, 5].
- We consider the ILC-250, 500, 1000, corresponding to the beam energy  $E_{beam} = 125, 250, 500$  GeV.

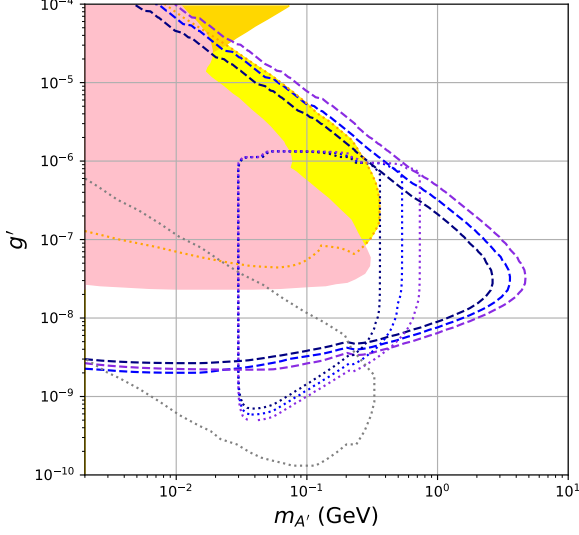
Notice that the shield length directly affects the sensitivity. With longer shield, the sensitivity to the short-lived LGB becomes worse.

## 5.1 $U(1)_{L_e-L_\mu}$ , $U(1)_{L_e-L_\tau}$ Models

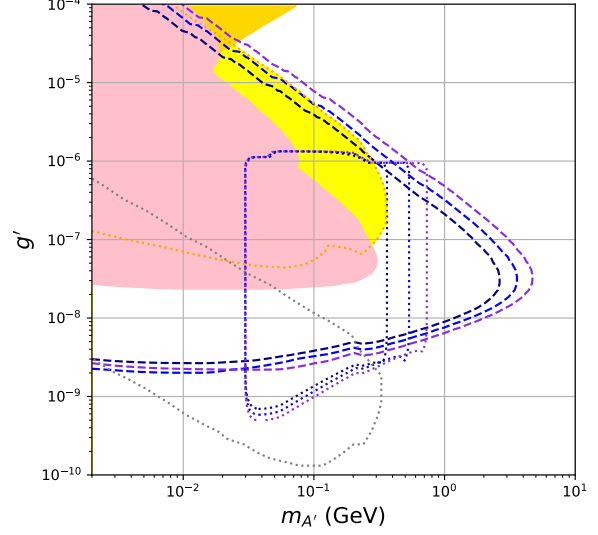
In Figs. 6 and 7, we show the contours of the number of signal events being equal to 3, which we call the discovery reaches. In Fig. 8, we also show the acceptance (*i.e.*, the ratio of the number of LGBs produced in the dump to the number of signals) of the  $U(1)_{L_e-L_\mu}$  model on  $m_{A'}-g'$  plane for the bremsstrahlung and annihilation processes. In Figs. 6 and 7, the yellow-shaded region is the expected sensitivity of the SHiP experiment, a future proton beam dump experiment [44]. For the LGB search, the  $e^\pm$  beam dump experiment has an advantage compared with the proton beam dump experiment. Since the LGBs of  $U(1)_{L_e-L_\mu}$  and  $U(1)_{L_e-L_\tau}$  models couple to the quarks only via the loop-suppressed kinetic mixing, the sensitivity of hadronic beam dump experiments is worse than the  $e^\pm$  case. This is the reason why the ILC beam dump experiment has better sensitivity than the SHiP experiment. We can see that the ILC beam dump experiment has a sensitivity to the unexplored region.

We comment on the behavior of the discovery reach. The sensitivity becomes worse as the coupling constant  $g'$  becomes too large or too small. In the large  $g'$  case, the LGBs are abundantly produced but most of them decays before reaching to the decay volume. The behavior of the discovery reach in the large coupling region can be understood from the fact that the decay probability depends exponentially on the combination  $\frac{m_{A'}^2 g'^2}{E_{A'}}$ , with  $E_{A'}$  being the energy of the LGB. In the bremsstrahlung process,  $E_{A'}$  does not depend on  $m_{A'}$  and  $g'$ , so the upper edge is along  $m_{A'} g' \sim \text{const.}$ . In the annihilation process,  $E_{A'} = \frac{m_{A'}^2}{2m_e}$  and contour is along  $g' \sim \text{const.}$ . In the small  $g'$  region, the production rate of LGB in the dump and the decay probability in the decay volume are both suppressed. The number of events is proportional to  $g'^4$  in the bremsstrahlung process and  $\frac{g'^4}{m_{A'}^2}$  in the annihilation process.<sup>#9</sup> We also comment that the sensitivity region of the annihilation process is sharply terminated at high and low values of the LGB mass. In the annihilation process,  $\sqrt{2m_e E_{e^+}} = m_{A'}$  holds

<sup>#9</sup>In our calculation, we set the lower limit of  $E_{A'}$  integral by  $m_{A'}$ , instead of  $E_{cut}$ . This induces the  $m_{A'}$  dependence to the bremsstrahlung sensitivity [41, 39]. Moreover, the number of produced LGB from the annihilation process depends on  $E_e$  because the track length depends on  $E_e$  [12]. This behavior is valid when  $E_e \sim E_{beam}$ .



(a) electron beam



(b) positron beam

Figure 6: The ILC beam dump experiment discovery reach for 10 years operation for the  $U(1)_{Le-L\mu}$  model. Left (right) figure shows the result with electron (positron) beam. Line colors correspond to the beam energy: 125 GeV (navy), 250 GeV (blue) and 500 GeV (purple). Line styles correspond to the production process: bremsstrahlung (dashed line) and annihilation (dotted line). The pink-shaded region is excluded by the previous beam dump experiments [41]. The orange-shaded region is excluded by the electron-neutrino scattering experiment, Texono [43]. The grey-shaded region is excluded by the observation of the supernova [28]. The yellow-shaded region is the expected sensitivity of the SHiP experiment [44].

under the narrow-width approximation. Then,  $E_{e^+} < E_{beam}$  sets an upper bound on  $m_{A'}$  which is kinematically accessible with the annihilation process. For the ILC-250, for example, the upper bound is about 300 MeV. This limit makes the right edge of the sensitivity region from the annihilation production. The left edge is from the LGB-mass dependence of  $E_{A'}$ . As we consider smaller  $m_{A'}$ , the energy of the LGB produced by the annihilation process becomes lower. Because the angle  $\theta_1$  of the positron becomes larger as the positron energy becomes smaller (see Eq. (4.14)), the annihilation process loses the sensitivity in the low mass region. This sets the left edge of the discovery reach from the annihilation process.

Comparing Figs. 6 and 7, the discovery reaches for the  $U(1)_{Le-L\mu}$  and  $U(1)_{Le-L\tau}$  models are similar. This is because the LGBs of both models directly couple to the electron. On the other hand, the dominant (visible) decay modes of the LGB are different. For the case of  $U(1)_{Le-L\mu}$ , the dominant visible decay modes are  $A' \rightarrow e^+e^-$  and  $\mu^+\mu^-$ , while the LGB of the  $U(1)_{e-\tau}$  model decays mostly into  $e^+e^-$  (if  $m_X < 2m_\tau$ ). These features may be used

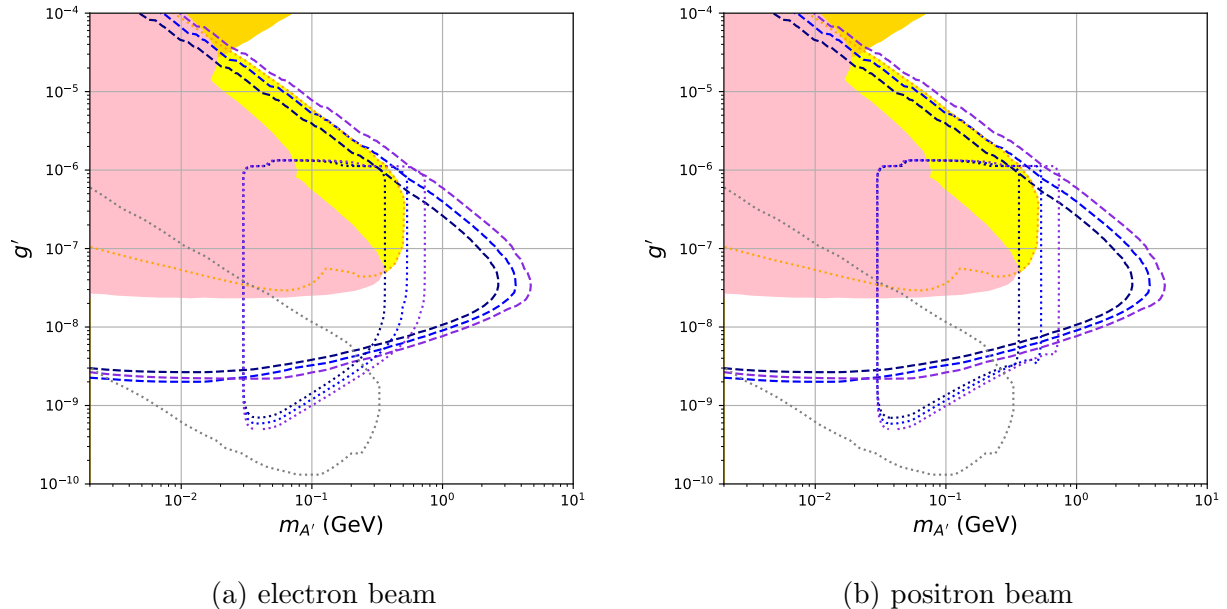


Figure 7: Same to Fig. 6, but for the  $U(1)_{L_e-L_\tau}$  model.

to distinguish the models behind the LGB, as discussed in Ref. [13].

## 5.2 $U(1)_{L_\mu-L_\tau}$ Model

Fig. 9 shows the discovery reach for the LGB in the  $U(1)_{L_\mu-L_\tau}$  model in the ILC-250 beam dump experiment with a 10-year operation. In addition to the  $e^\pm$  bremsstrahlung and the annihilation production processes, we also consider the muon bremsstrahlung production process.<sup>#10</sup> The muon bremsstrahlung process is important for the  $U(1)_{L_\mu-L_\tau}$  model because the LGB directly couples to muon. We can see that the ILC beam dump experiment has a sensitivity to the region which has not been excluded yet. Particularly, the LGB in the  $U(1)_{L_\mu-L_\tau}$  model is motivated by the fact that it may alleviate the Hubble tension [28]. The ILC beam dump experiment can access the part of the region suggested by the Hubble tension.

In the previous study of the search of the LGBs with the ILC beam dump experiment [13], only the production process by the beam particle was considered. We can see that the effects of the secondary particles extend the sensitivity to the small-coupling region and that

<sup>#10</sup>For the  $U(1)_{L_e-L_\mu}$  model, muon bremsstrahlung process contributes to the sensitivity without loop-suppression. Electron bremsstrahlung process, however, also contributes to the sensitivity without loop-suppression in this model. Since the number of initial electrons is much larger than the number of initial muons in the electron beam dump experiment, the contributions from the muon bremsstrahlung process are expected to be much smaller than the contributions from electrons. The yellow regions show the expected sensitivity of the SHiP experiment [44].

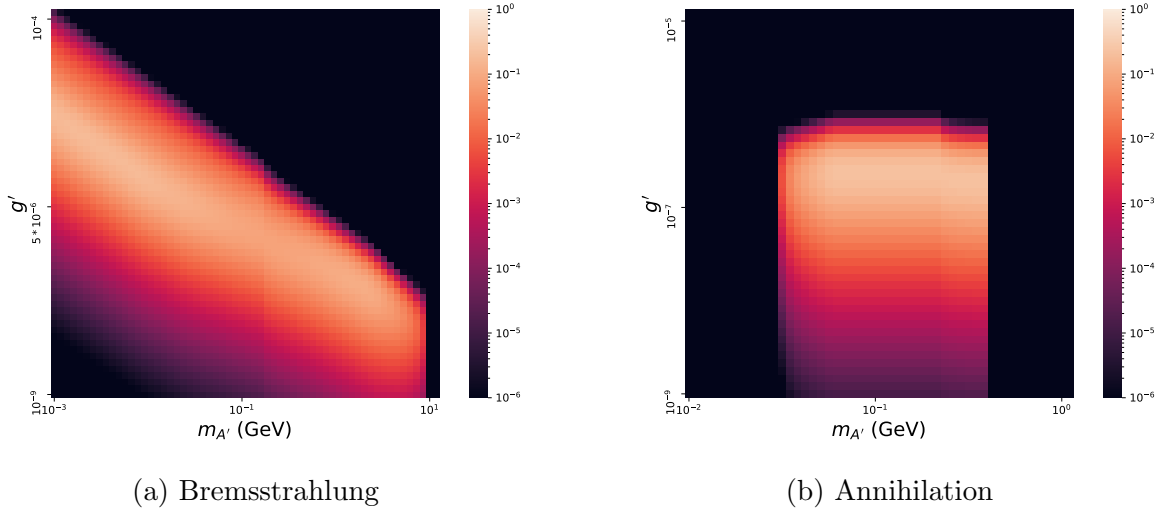


Figure 8: Heatmap of the acceptance (*i.e.*, the ratio of the number of LGBs produced in the dump to the number of signals) on  $m_{A'}-g'$  plane. In this figure, we consider the LGB associated with  $U(1)_{L_e-L_\mu}$ , but the behavior is not so different when we consider the other models.

the muon bremsstrahlung effects extend the sensitivity to the large-mass region. Due to the large cross section and the different kinematics, we can also see that the signal produced by the annihilation process may cover the parameter region uncovered by the bremsstrahlung process. The annihilation process requires the positron in the initial state. For better sensitivity from the annihilation production, the use of a positron beam is better.

## 6 The Muon Beam Dump Experiment

In this section, we consider the beam dump experiment using a muon beam at the muon collider.<sup>#11</sup> The muon beam dump experiment has advantages to search for muon-philic new particles. In particular, in the  $U(1)_{L_\mu-L_\tau}$  model, the LGB does not couple to electron at tree level and then the production cross section is suppressed in the  $e^\pm$  beam dump experiment. We expect that the muon beam dump experiment has a good sensitivity to the LGB in the  $U(1)_{L_\mu-L_\tau}$  model. Thus, in this section, we study the search of the LGB in the  $U(1)_{L_\mu-L_\tau}$  model at the muon beam dump experiment. Such a subject was already considered in Ref. [10]. In the paper, however, the effect of the loop-induced kinetic mixing was not taken into account, so the sensitivity below the di-muon mass was underestimated. In the present study, the loop-induced kinetic mixings is included in deriving the discovery reach.

We consider the experimental setup similar to the one in the  $e^\pm$  beam dump experiment. We consider a lead target as well as a water target for comparison; the length of the target

<sup>#11</sup>Since muons are not stopped by the target, the target is not a beam dump. We, however, call the experiment as “beam-dump experiment” as we did in the case of  $e^+e^-$  colliders.



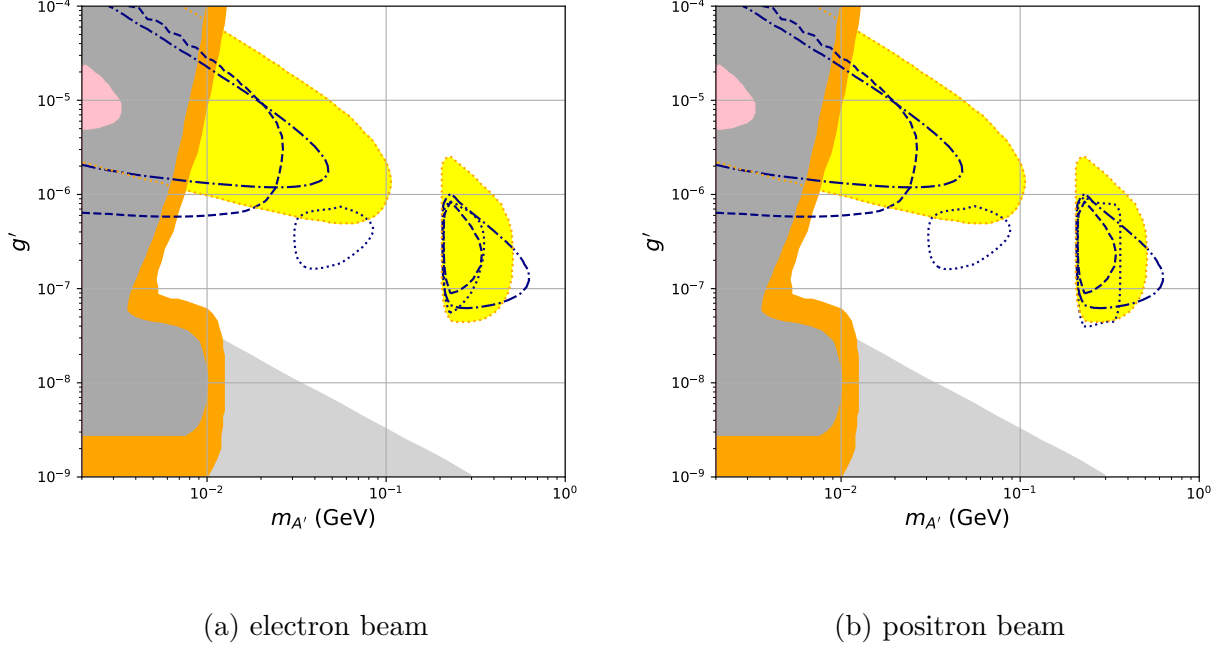


Figure 9: The  $e^\pm$  beam dump experiment discovery reach for the  $U(1)_{L_\mu-L_\tau}$  extension model. Several production processes of the LGB are considered:  $e$  bremsstrahlung (dashed line),  $\mu$  bremsstrahlung (dash-dotted line), and the annihilation (dotted line). The pink shaded region is excluded by the previous beam dump experiment, E137 at SLAC [45, 41]. The dark gray region is excluded by the BBN constraint [46]. The light grey shaded region is excluded by the observation of SN1987A [28]. In the orange-shaded region, the Hubble tension is alleviated [28].

is taken to be 11 m. Then, the shield and the decay volume with the detectors are assumed to be installed behind the target. As a source of the muon beam, we consider the US Muon Accelerator Program (MAP) design, where the number of muons in the beam is  $N_\mu \sim 10^{20}$  per year and the beam energy is 1.5 TeV [49]. In the muon beam dump experiment based on the MAP, the muons in the beam are very energetic and we may have serious muon background. In the SHiP experiment, for example, the muons with the energy  $\sim 400$  GeV are expected to be removed by 50 m active shield. With rescaling this result, 1.5 TeV muons may be removed by using  $\sim 200$  m active shield; we take  $L_{shield} = 200$  m as our canonical value of the shield length. We also consider the cases with shorter shield length which may be realized if a stronger magnet or additional technical progresses are developed in the future.

As the event rate in the  $e^\pm$  beam dump experiment, the event rate in the muon beam dump experiment can be estimated as

$$N = B_{vis} N_\mu \frac{N_{Avo} \rho}{A} \int_{m_\mu + m_{A'}}^{E_{beam}} dE_\mu \int_{m_{A'}}^{E_\mu - m_e} dE_{A'} \frac{dl_\mu}{dE_\mu} \frac{1}{E_\mu} \left[ \frac{d\sigma}{dx} \right]_{x=\frac{E_{A'}}{E_\mu}} \mathcal{A}_\mu \Theta(L_{dump} - \delta_\mu). \quad (6.1)$$

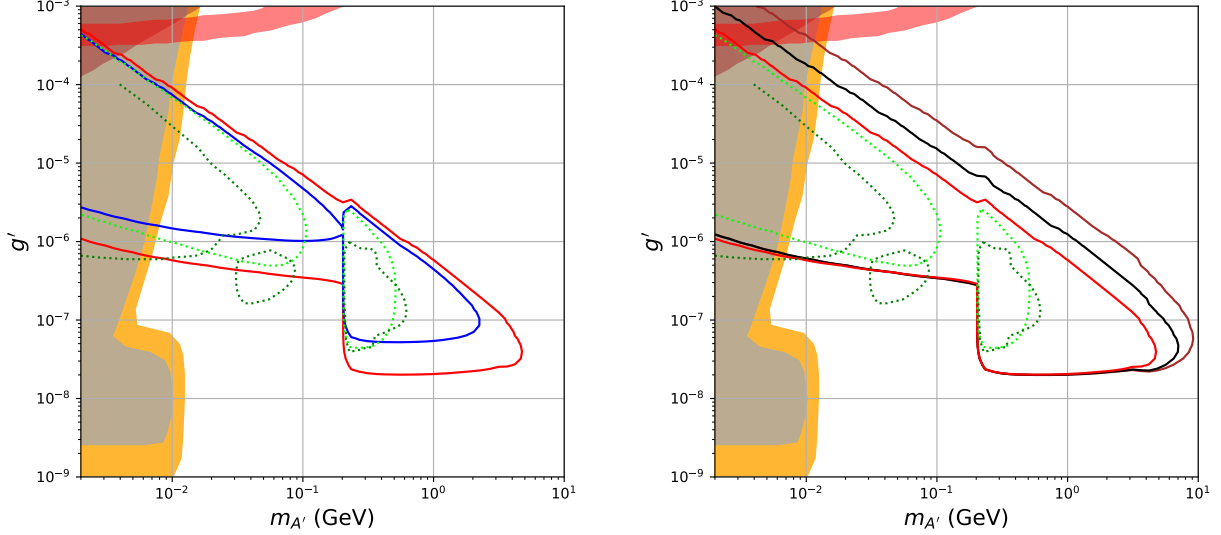


Figure 10: The muon beam dump experiment discovery reach for the case of  $U(1)_{L_\mu-L_\tau}$  extension model (solid lines). The grey-shaded (brown-shaded) region is excluded by the BBN observation [28] (the solar neutrino observation [47, 48]). In the orange-shaded region, the Hubble tension is alleviated by the LGB [28]. The red-shaded region is the one motivated by the muon  $g-2$  anomaly. The green (light green) dotted line shows the expected discovery reach in the ILC beam dump experiment (SHiP experiment), as shown in Sec. 5. The left figure shows the case with 200 m shield and lead (red) or water (blue) target. The right figure shows the case with lead target and several length shield: 200 m (red), 50 m (brown), and 10 m (black).

For the calculation of the acceptance  $\mathcal{A}_\mu$ , we take  $\theta_1 = \theta_0$  (see Eq. (4.20)) and we obtain

$$\mathcal{A}_\mu \simeq e^{-(L_{dump}+L_{shield}-\delta_\mu)/L_{A'}} (e^{-z_{min}/L_{A'}} - e^{-L_{dec}/L_{A'}}), \quad (6.2)$$

where

$$z_{min} = \frac{1}{\theta_3} [-\theta_2 \delta_\mu + (\theta_1 + \theta_2)(L_{dump} + L_{shield}) + (\theta_1 + \theta_2 + \theta_3)L_{dec} - r_{det}].$$

The theta function in Eq. (6.1) takes care of the fact that the muons do not stop in the dump.<sup>#12</sup> Notice that  $\theta_1$  and  $z_{min}$  are calculated by using the fact that the initial-state muon is the beam particle not the secondary one.

Fig. 10 shows the discovery reach for the LGB in the  $U(1)_{L_\mu-L_\tau}$  model with the muon beam dump experiment based on the MAP. For the case of the  $U(1)_{L_\mu-L_\tau}$  model, we can

<sup>#12</sup>In this setup, we assume the shield is active, that is, muons will be removed by the magnetic field. Then the muon does not produce the LGB in the shield.

see that the muon beam dump experiment has better sensitivity than the future electron and proton beam dump experiments, especially for the case of large LGB mass. We can see that the muon beam dump experiment can access the parameter region suggested by the Hubble tension. Unfortunately, the muon beam dump experiment hardly reach the region explaining the muon  $g - 2$  anomaly.

## 7 Summary and Discussion

In this paper, we have discussed the possibility to search for the LGBs in the lepton beam dump experiments. In the  $e^\pm$  beam dump experiment, we calculate the event rate taking into account the effects of the secondary particles which were not considered in the previous study [13]. Then we consider the production processes not only the electron bremsstrahlung but also the annihilation process and the muon bremsstrahlung process. Since the annihilation process has fewer vertices than the bremsstrahlung process, the cross section tends to be larger than that of the bremsstrahlung process. We have shown that these new production processes extend the discovery reaches for the LGB (see Fig. 6 – 10). We also considered the search for the LGB of the  $U(1)_{L_\mu-L_\tau}$  model in the muon beam dump experiment. We include the effect of the loop-induced kinetic mixing, which was not considered in the previous work [10]. For muon-philic particles, in particular, the LGB of the  $U(1)_{L_\mu-L_\tau}$  model, the muon beam dump experiment gives a better sensitivity than the electron ones.

There are the other LGB production processes, for example, the decay of hadrons. Hadrons can be produced in the lepton beam dump via the photoproduction processes [50] and then the some of hadrons decay into the LGB. This process may extend the sensitivity as in the SHiP experiment. Such an issue will be discussed in elsewhere.

*Acknowledgments:* The work was supported by JSPS KAKENHI Grant No. 16H06490 (TM), 18K03608 (TM) and 22H01215 (TM), 22J21016 (AN).

## References

- [1] T. Behnke, J.E. Brau, B. Foster, J. Fuster, M. Harrison, J.M. Paterson et al., eds., *The International Linear Collider Technical Design Report - Volume 1: Executive Summary*, 1306.6327.
- [2] H. Baer et al., eds., *The International Linear Collider Technical Design Report - Volume 2: Physics*, 1306.6352.
- [3] C. Adolphsen et al., eds., *The International Linear Collider Technical Design Report - Volume 3.I: Accelerator \& in the Technical Design Phase*, 1306.6353.
- [4] C. Adolphsen et al., eds., *The International Linear Collider Technical Design Report - Volume 3.II: Accelerator Baseline Design*, 1306.6328.

- [5] H. Abramowicz et al., *The International Linear Collider Technical Design Report - Volume 4: Detectors*, 1306.6329.
- [6] ILC INTERNATIONAL DEVELOPMENT TEAM collaboration, *The International Linear Collider: Report to Snowmass 2021*, 2203.07622.
- [7] CLIC, CLICDP collaboration, P. Roloff, R. Franceschini, U. Schnoor and A. Wulzer, eds., *The Compact Linear  $e^+e^-$  Collider (CLIC): Physics Potential*, 1812.07986.
- [8] J.P. Delahaye, M. Diemoz, K. Long, B. Mansoulié, N. Pastrone, L. Rivkin et al., *Muon Colliders*, 1901.06150.
- [9] S. Kanemura, T. Moroi and T. Tanabe, *Beam dump experiment at future electron-positron colliders*, *Phys. Lett. B* **751** (2015) 25 [1507.02809].
- [10] C. Cesarotti, S. Homiller, R.K. Mishra and M. Reece, *Probing New Gauge Forces with a High-Energy Muon Beam Dump*, 2202.12302.
- [11] Y. Sakaki and D. Ueda, *Searching for new light particles at the international linear collider main beam dump*, *Phys. Rev. D* **103** (2021) 035024 [2009.13790].
- [12] K. Asai, S. Iwamoto, Y. Sakaki and D. Ueda, *New physics searches at the ILC positron and electron beam dumps*, 2105.13768.
- [13] K. Asai, T. Moroi and A. Niki, *Leptophilic Gauge Bosons at ILC Beam Dump Experiment*, *Phys. Lett. B* **818** (2021) 136374 [2104.00888].
- [14] R. Foot, *New Physics From Electric Charge Quantization?*, *Mod. Phys. Lett. A* **6** (1991) 527.
- [15] X.G. He, G.C. Joshi, H. Lew and R.R. Volkas, *NEW Z-prime PHENOMENOLOGY*, *Phys. Rev. D* **43** (1991) 22.
- [16] X.-G. He, G.C. Joshi, H. Lew and R.R. Volkas, *Simplest Z-prime model*, *Phys. Rev. D* **44** (1991) 2118.
- [17] R. Foot, X.G. He, H. Lew and R.R. Volkas, *Model for a light Z-prime boson*, *Phys. Rev. D* **50** (1994) 4571 [hep-ph/9401250].
- [18] T. Araki, J. Heeck and J. Kubo, *Vanishing Minors in the Neutrino Mass Matrix from Abelian Gauge Symmetries*, *JHEP* **07** (2012) 083 [1203.4951].
- [19] J. Heeck, *Neutrinos and Abelian Gauge Symmetries*, Ph.D. thesis, Heidelberg U., 2014.
- [20] K. Asai, K. Hamaguchi and N. Nagata, *Predictions for the neutrino parameters in the minimal gauged  $U(1)_{L_\mu-L_\tau}$  model*, *Eur. Phys. J. C* **77** (2017) 763 [1705.00419].

- [21] K. Asai, K. Hamaguchi, N. Nagata, S.-Y. Tseng and K. Tsumura, *Minimal Gauged  $U(1)_{L_\alpha-L_\beta}$  Models Driven into a Corner*, *Phys. Rev. D* **99** (2019) 055029 [1811.07571].
- [22] K. Asai, *Predictions for the neutrino parameters in the minimal model extended by linear combination of  $U(1)_{L_e-L_\mu}$ ,  $U(1)_{L_\mu-L_\tau}$  and  $U(1)_{B-L}$  gauge symmetries*, *Eur. Phys. J. C* **80** (2020) 76 [1907.04042].
- [23] E. Ma and D.P. Roy, *Anomalous neutrino interaction, muon  $g-2$ , and atomic parity nonconservation*, *Phys. Rev. D* **65** (2002) 075021 [hep-ph/0111385].
- [24] S. Baek, N.G. Deshpande, X.G. He and P. Ko, *Muon anomalous  $g-2$  and gauged  $L(\text{muon}) - L(\text{tau})$  models*, *Phys. Rev. D* **64** (2001) 055006 [hep-ph/0104141].
- [25] P. Foldenauer, *Light dark matter in a gauged  $U(1)_{L_\mu-L_\tau}$  model*, *Phys. Rev. D* **99** (2019) 035007 [1808.03647].
- [26] I. Holst, D. Hooper and G. Krnjaic, *The Simplest and Most Predictive Model of Muon  $g - 2$  and Thermal Dark Matter*, 2107.09067.
- [27] M. Drees and W. Zhao,  *$U(1)_{L_\mu-L_\tau}$  for Light Dark Matter,  $g_\mu - 2$ , the 511 keV excess and the Hubble Tension*, 2107.14528.
- [28] M. Escudero, D. Hooper, G. Krnjaic and M. Pierre, *Cosmology with A Very Light  $L_\mu - L_\tau$  Gauge Boson*, *JHEP* **03** (2019) 071 [1901.02010].
- [29] LDMX collaboration, *Light Dark Matter eXperiment (LDMX)*, 1808.05219.
- [30] V.V. Ezhela, S.B. Lugovsky and O.V. Zenin, *Hadronic part of the muon  $g-2$  estimated on the  $\sigma^{**2003}(\text{tot})(e^+ e^- \rightarrow \text{hadrons})$  evaluated data compilation*, hep-ph/0312114.
- [31] PARTICLE DATA GROUP collaboration, *Review of Particle Physics*, *PTEP* **2020** (2020) 083C01.
- [32] SHiP collaboration, *The active muon shield in the SHiP experiment*, *JINST* **12** (2017) P05011 [1703.03612].
- [33] K.J. Kim and Y.-S. Tsai, *IMPROVED WEIZSACKER-WILLIAMS METHOD AND ITS APPLICATION TO LEPTON AND W BOSON PAIR PRODUCTION*, *Phys. Rev. D* **8** (1973) 3109.
- [34] Y.-S. Tsai, *Pair Production and Bremsstrahlung of Charged Leptons*, *Rev. Mod. Phys.* **46** (1974) 815.
- [35] Y.-S. Tsai, *AXION BREMSSTRAHLUNG BY AN ELECTRON BEAM*, *Phys. Rev. D* **34** (1986) 1326.

- [36] D.V. Kirpichnikov, H. Sieber, L.M. Bueno, P. Crivelli and M.M. Kirsanov, *Probing hidden sectors with a muon beam: Total and differential cross sections for vector boson production in muon bremsstrahlung*, *Phys. Rev. D* **104** (2021) 076012 [2107.13297].
- [37] Y.-S. Liu, D. McKeen and G.A. Miller, *Validity of the Weizsäcker-Williams approximation and the analysis of beam dump experiments: Production of a new scalar boson*, *Phys. Rev. D* **95** (2017) 036010 [1609.06781].
- [38] Y.-S. Liu and G.A. Miller, *Validity of the Weizsäcker-Williams approximation and the analysis of beam dump experiments: Production of an axion, a dark photon, or a new axial-vector boson*, *Phys. Rev. D* **96** (2017) 016004 [1705.01633].
- [39] A. Niki, *New Gauge Bosons at ILC Beam Dump Experiment*, *Master Thesis* (2022) .
- [40] J.D. Bjorken, R. Essig, P. Schuster and N. Toro, *New Fixed-Target Experiments to Search for Dark Gauge Forces*, *Phys. Rev. D* **80** (2009) 075018 [0906.0580].
- [41] M. Bauer, P. Foldenauer and J. Jaeckel, *Hunting All the Hidden Photons*, *JHEP* **07** (2018) 094 [1803.05466].
- [42] Y. Sakaki, Y. Namito, T. Sanami, H. Iwase and H. Hirayama, *Implementation of muon pair production in PHITS and verification by comparing with the muon shielding experiment at SLAC*, *Nucl. Instrum. Meth. A* **977** (2020) 164323 [2004.00212].
- [43] TEXONO collaboration, *Measurement of  $Nu(e)\text{-}\bar{\nu}_e$ -Electron Scattering Cross-Section with a CsI(Tl) Scintillating Crystal Array at the Kuo-Sheng Nuclear Power Reactor*, *Phys. Rev. D* **81** (2010) 072001 [0911.1597].
- [44] S. Alekhin et al., *A facility to Search for Hidden Particles at the CERN SPS: the SHiP physics case*, *Rept. Prog. Phys.* **79** (2016) 124201 [1504.04855].
- [45] J.D. Bjorken, S. Ecklund, W.R. Nelson, A. Abashian, C. Church, B. Lu et al., *Search for Neutral Metastable Penetrating Particles Produced in the SLAC Beam Dump*, *Phys. Rev. D* **38** (1988) 3375.
- [46] A. Kamada and H.-B. Yu, *Coherent Propagation of PeV Neutrinos and the Dip in the Neutrino Spectrum at IceCube*, *Phys. Rev. D* **92** (2015) 113004 [1504.00711].
- [47] G. Bellini et al., *Precision measurement of the  ${}^7\text{Be}$  solar neutrino interaction rate in Borexino*, *Phys. Rev. Lett.* **107** (2011) 141302 [1104.1816].
- [48] Y. Kaneta and T. Shimomura, *On the possibility of a search for the  $L_\mu - L_\tau$  gauge boson at Belle-II and neutrino beam experiments*, *PTEP* **2017** (2017) 053B04 [1701.00156].

- [49] J.-P. Delahaye et al., *Enabling Intensity and Energy Frontier Science with a Muon Accelerator Facility in the U.S.: A White Paper Submitted to the 2013 U.S. Community Summer Study of the Division of Particles and Fields of the American Physical Society*, in *Community Summer Study 2013: Snowmass on the Mississippi*, 8, 2013 [1308.0494].
- [50] P. Schuster, N. Toro and K. Zhou, *Probing invisible vector meson decays with the NA64 and LDMX experiments*, *Phys. Rev. D* **105** (2022) 035036 [2112.02104].